Magnetic Hyperthermia to Promote Acrylamide Radical Polymerizations

Magnetic hyperthermia to promote acrylamide radical polymerizations

Marta Vassallo,[a] Marta Vicentini,[a] Martina Salzano De Luna,[b] Gabriele Barrera,[a] Paola Tiberto,[a] Alessandra Manzin,[a] Daniele Martella [a,b,c,]*

[a] Istituto Nazionale di Ricerca Metrologica (INRiM), Strada delle Cacce 91, 10135 Torino, Italy.

[b] Department of Chemical, Materials and Industrial Production Engineering – University of Naples Federico II, Piazzale V. Tecchio, 80, 80125 Napoli, Italy

[c] European Laboratory for Non Linear Spectroscopy (LENS), Via N. Carrara 1, 50019 Sesto Fiorentino, Firenze, Italy. E-mail: martella@lens.unifi.it

[d] Department of Chemistry "Ugo Schiff", University of Florence, Via N. Carrara 3-13, 50019 Sesto Fiorentino, Italy. E-mail: daniele.martella@unifi.it

KEYWORDS. magnetic hyperthermia, cobalt ferrite nanoparticles, free radical polymerizations, magnetic hydrogels, polyacrylamides

ABSTRACT

Radical polymerization is widely employed for the preparation of advanced materials with controlled properties and responsiveness. Depending on the radical initiator, different stimuli can trigger the beginning of the reaction. This work presents an innovative approach that exploits the

heat released by magnetic nanoparticles when excited by an alternating current (AC) magnetic field to induce radical polymerizations. In particular, the use of cobalt ferrite ($CoFe_2O_4$) nanoparticles is explored for the preparation of polyacrylamide hydrogels, chosen as model material to demonstrate the effectiveness of the proposed technique. Magnetic and mechanical characterizations reveal that the obtained materials possess properties similar to those of samples prepared by classical thermal polymerization. Indeed, magnetic hyperthermia is a versatile tool for remote temperature control in a localized space that can find different applications. An example is represented by its use for the selective volume polymerization in a thermo-sensitive environment, overcoming classical problems of both bulk thermal polymerization (e.g. not applicable in delicate environments) and photopolymerization (e.g. poor light penetration). The obtained results pave the way also for production of non-magnetic materials, in which magnetic nanoparticles are first concentrated in a small solution volume (by a permanent magnet) and then exploited to activate the polymerization of the whole material (by an AC magnetic field).

1. Introduction

Radical polymerizations allow to obtain a widespread variety of materials for applications that span from biology to technological and industrial production. [1] Despite the huge diversity of the materials obtained, all radical polymerization processes involve at least a monomer, with suitable functional groups (e.g. acrylate, vinyl), and a radical initiator. [2] The latter species produce free radicals by decomposition in selected conditions, eventually starting a cascade process to form the polymeric chain. In fact, the initial radical adds to a monomer unit, thus growing the polymer chain and forming new radical species that, in turn, can add to other monomers.

Initiation is a critical parameter to determine the final polymer properties: indeed, using the same monomer formulations, the material structure can be tuned by different reaction conditions. [3-5] The most common methods to induce radical polymerization employ initiators that produce radicals under heating ("thermal polymerization") or light irradiation ("photopolymerization"). [6] The main advantage of both methodologies are summarized in **Figure 1a**. Other initiation systems can include electrolysis, [7] microwaves [8] or ultrasound application. [9-11]

Classical thermal heating is the easiest way to achieve radical polymerization and to obtain bulk materials without requiring specialized instruments/reactors (e.g. it uses heating plates, ovens). [8] On scaling up the polymerization process, some issues arise because of the inevitable thermal gradient in the material volume during the polymerization process, which can lead to material inhomogeneity. On the other hand, photopolymerization is a very appealing strategy to confine the reaction in a specific volume (where light is shined), opening to be used from large area coatings to photolithographic techniques (with resolution up to the nanometer scale). [12-14] Photopolymerization can be directly employed to 3D shape polymeric materials [15-16] and in biological environments, by appropriate choice of the photoinitiator and activating wavelength. [17] In turn, this method suffers from poor light penetration inside the monomeric formulation and need of transparent environment, thus limiting the size and composition of monomers and the type of substrate/vessel where the process is triggered.

Some limitations of both strategies find a solution in the so-called frontal polymerization, which is activated only by applying a local stimulus to the monomer solution (either heating or irradiation) and then, it is self-sustained through the whole volume by the heat released locally during the radical addition. [18-20] A wireless control on the reaction is not possible since a

physical contact between the monomer formulation and a radical activator source (light or any heaters) is needed to start the process.

All these methods still lack versatility. More specifically, the possibility to obtain bulk material, spatial selectivity and *in situ* process in an opaque (even biological) environment, are features that are still difficult to combine with all the aforementioned techniques.

To achieve these objectives, previous reports showed the application of indirect heating strategies like electromagnetic induction, [21,22] in which, for example, the polymerization is started by a pulsed magnetic field, thanks to the action of susceptor and resistive heating elements inserted in the monomeric formulation, e.g. metallic additives, metal grids. [23] Another versatile system to realize wireless mode heating is based on the use of magnetic nanoparticles (MNPs), which can release heat mainly via hysteresis losses, when excited by alternating current (AC) magnetic fields. [24,25] This phenomenon, known as magnetic hyperthermia, is mainly studied in the biomedical field and, in particular, in cancer treatment, where it is used to selectively increase the tumor temperature up to 40-45 °C, in order to cause an increased sensitivity of cancer cells to other therapies, such as chemotherapy or radiotherapy. [26] This technique relies on the injection of MNPs in the tumor area, and in their activation with an AC magnetic field with frequency typically in the range from 50 kHz to 1 MHz. Depending on their physicochemical and dimensional properties (i.e. composition, surface coating, size, shape, and state of aggregation), MNPs demonstrate a different efficiency in heat generation, which is usually expressed by the specific loss power (SLP), i.e. the power dissipated per unit mass of magnetic material. [27,28]

In the framework of polymeric material technologies, MNPs find also some interesting applications, being used to heat the system and control the shape of shape-memory composites,

[29,30] activate self-healing [31,32] or even induce crosslinking reactions in polyimides [33] or polydimethylsiloxanes. [34] Moreover, magnetic hyperthermia has been applied to trigger radical polymerization directly on the (hot) surface of MNPs, to functionalize them and thus obtain functional micro/nano systems. [35,36] Even if the use of MNP-based heating to control radical polymerization is still limited, other effects due to MNPs chemical structure have been recently exploited to obtain bulk materials via acrylate monomer polymerization. First, MNPs capped with carboxylic acid derivatives have been demonstrated able to work as one-component photoinitiator under UV irradiation, even if the efficiency of the system has to be improved with a co-initiator (a tertiary amine) to be competitive with other photoactivated radical generators. [37] Second, MNPs can spontaneously mimic the enzymatic activity of peroxidase, [38] and have been used to mediate radical polymerization at room temperature starting from an aqueous solution once mixed with hydrogen peroxide (as radical sources decomposed by the nanoenzyme). [39]

At the end, the magnetic properties can be also directly used to selectively enhance the polymerization reaction yield in a specific region of a sample. In this case, MNPs have been functionalized with a copper-immobilized dendrimer able to induce the decomposition of tert-butyl peroxybenzoate which starts radical reactions. Thanks to the application of locally focused magnetic fields, the nano-co-initiator can be concentrated in a selected space to achieve the reaction only in a confined volume. [40]

In this article, we combine the potential advantages of all the aforementioned technologies exploiting magnetic hyperthermia to trigger the radical polymerization of acrylamide based monomers. $CoFe_2O_4$ NPs have been added to an aqueous acrylamide formulation that is polymerized under the application of a 100 kHz magnetic field. Indeed, magnetic hyperthermia has been used as an alternative non-contactless heating source with respect to classical thermal

polymerization, while the mechanism remains a standard free radical polymerization. The properties of the hydrogel obtained by this process have been compared with those of the hydrogel prepared by classical thermal polymerization. The heating-cooling transient during the polymerization process has been also numerically modeled, in order to further corroborate the combined action of AC magnetic fields and MNPs as precursors of the exothermic reaction at the basis of the radical polymerization. Moreover, the modeling approach has been used to explore the capability of different types of MNPs to promote the reaction, as a function of their heating properties. As a proof of concept of the versatility of our approach, we also demonstrate how the technology can be employedin delicate (thermo-sensitive) environments or extended to non-magnetic materials, exploiting the diffusion of heat produced by the MNPs only in a localized part of the sample.

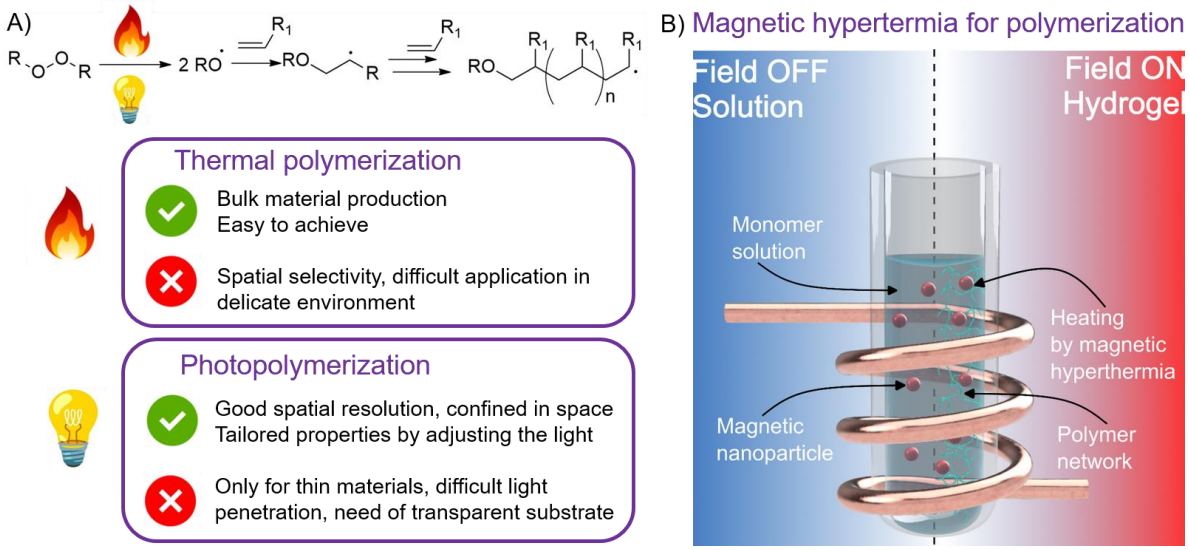

Figure 1. Strategies to trigger radical polymerizations. A) General reaction of a free radical polymerization and main feature of thermal or photo-activated processes; B) Schematic of magnetic hyperthermia to activate a radical polymerization.

2. Experimental part

2.1. Synthesis of magnetic nanoparticles. $CoFe_2O_4$ NPs were synthesized through the co-precipitation method. [41] Briefly, cobalt(II) nitrate hexahydrate (2.8 g) and iron(III) chloride hexahydrate (5.4 g) were dissolved in deionized water (300 mL). Under vigorous stirring, an aqueous solution of sodium hydroxide (10 M) was added to reach a pH of 13. The reaction mixture was heated to 100 °C, under stirring and nitrogen flow, and iron(III) nitrate nonahydrate (3.9 g) was added to the solution after 30 min; the reaction was carried on for another 30 min. After cooling to room temperature, the precipitate obtained was magnetically decanted and washed several times using deionized water up to neutral pH. The methods for nanoparticle characterization are reported in Supporting Information.

2.2. Hydrogel preparation. Hydrogel monomer formulation was prepared by dissolving 200 mg of acrylamide, 10 mg of bis-acrylamide, and 10 mg of ammonium persulfate in deionized water (final volume of 2 mL). For the magnetic hydrogel, an aqueous suspension of $CoFe_2O_4$ NPs with a concentration of 14 mg/mL was used instead of deionized water.

The hydrogel polymerization was induced in two different ways depending on the sample, as reported in Table 2. On the one hand, bulk heating was obtained by placing the sample in a water bath at 60 °C for 10 min, while on the other hand, the polymerization was induced by exposing the sample to an AC magnetic field with a peak amplitude of 40 kA/m and a frequency of 100 kHz for 7 min, exploiting the heating efficiency of $CoFe_2O_4$ NPs. All the polymerization was performed in glass cylindrical vials (internal diameter of 12 mm) or plastic cylindrical ones (internal diameter of 17 mm).

The thermo-responsive hydrogel was prepared by dissolving 1% w/w of ultra-low gelling point agarose in water at 80 °C and then cooled down at room temperature to obtain gelation.

The methods for hydrogel characterization are reported in Supporting Information.

2.3. Heat transfer numerical modeling. The heating-cooling transient occuring in the magnetic gel was simulated by means of an in-house 3D finite element solver. This solves the heat transfer equation under negligible convection phenomena within a system that comprises the magnetic gel, where MNPs are uniformly dispersed, the vial walls and the portion of air above the gel. [42] In particular, the following equation was implemented:

$$\rho C_p \frac{\partial T}{\partial t} = \nabla \cdot k\nabla T + \Gamma_1 Q_{MNPs} + \Gamma_2 Q_{reaction} \quad (1)$$

where T is the temperature, ρ is the density of the medium (magnetic gel, plastic vial or air), C_p is the medium heat capacity, k is the medium thermal conductivity, Q_{MNPs} is the specific heating power released by MNPs under the action of an AC magnetic field, and $Q_{reaction}$ is the specific heating power released by the exothermic reaction during the polymerization process. Specifically, Q_{MNPs} is defined as the product of the SLP (from thermometric measurements) and the MNP concentration within the sample, while $Q_{reaction}$ is derived from the measured reaction enthalpy. Γ_1 and Γ_2 are piecewise functions equal to 1 in the magnetic gel and zero elsewhere, in particular $\Gamma_1 \neq 0$ when the magnetic field is switched on and the MNPs result activated, while $\Gamma_2 \neq 0$ during the exothermic reaction.

Equation (1) is completed by the following boundary condition on the external surface of the vial:

$$q = -k \frac{\partial T}{\partial n} = -h(T_{ext} - T), \quad (2)$$

where q is the outward heat flux, h is the heat transfer coefficient, and T_{ext} is the external temperature, i.e. the room temperature.

The finite element solution of (1) was obtained by discretizing the domain of analysis into a tetrahedral mesh and employing linear shape functions; the time integration was performed by applying the Crank-Nicolson method.

Table 1 summarizes the material properties employed in the thermal simulations for the magnetic gel, the vial (made of polyethylene), and the air. The initial temperature of the system was assumed to be uniform in space and equal to the external temperature, set at 26.4 °C. The heat transfer coefficient is fixed to 25 W m^{-2} K^{-1}, [43] as a limit condition for free convection in air.

Table 1. Summary of the material properties used in the thermal simulations.

Material	**ρ** **[kg/m^3]**	C_p **[J/(kg K)]**	k **[W/(m K)]**
Hydrogel [44]	1024	6350	0.83
Polyethylene	950	1900	0.5
Air	1.16	1007	0.026

3. Results and Discussion

3.1. Assessment of radical polymerization via magnetic hyperthermia

The concept pursued in this article to obtain a radical polymerization by magnetic hyperthermia is depicted in Figure 1b. The formulation was composed of a standard mixture of monomers (in our study acrylamide based molecules) dissolved in a solvent with a thermal initiator. A specific

amount of MNPs was added to this composition, in order to locally release heat after the application of an AC magnetic field, and thus start the polymerization under controlled conditions.

The first critical step is the selection of the type of MNPs. In fact, by changing material composition, size and shape it is possible to modulate the MNP heating efficiency, and obtain optimal SLP values for specific frequencies and peak amplitudes of the exciting magnetic field. In particular, many studies have demonstrated that it is possible to achieve a high heating efficiency of the MNPs by finely tuning their magnetocrystalline anisotropy [45-48] and/or shape anisotropy, [45-47,49,50] even if the synthesis of MNPs with well-controlled geometry requires thermal decomposition at high temperature and/or high pressure. [50] On the other hand, in our study we focused on MNPs that can be synthesized easily in the gram scale. Recently, we optimized a recipe for the production of Fe_3O_4 NPs by co-precipitation method, demonstrating that both the synthesis parameter (e.g. temperature) and possible surface coating can be exploited to improve colloidal stability and hyperthermia properties. [28] Here, a similar protocol was adapted for $CoFe_2O_4$ NPs, reaching satisfactory heating properties. Briefly, the MNPs were prepared with a co-precipitation method, by adding a basic NaOH solution to a solution containing cobalt(II) and iron(III) salts. The synthesis was scaled up to 2.5 g of MNPs, which were then characterized in terms of dimensional, magnetic and heating properties, as reported in **Figure 2**.

A representative TEM image of the $CoFe_2O_4$ NPs is shown in Figure 2A. The MNPs have a spherical shape and a quite uniform size distribution, as demonstrated by the histogram reported in Figure 2B, obtained from a statistical analysis of the TEM image. The MNPs have a mean diameter of 13.7 nm and a standard deviation of 1.2 nm. Figure 2C displays the magnetization curve *M-H* of the MNPs, measured at room temperature. The *M-H* curve was normalized to the mass of the magnetic material, and the saturation magnetization value results to be approximately

52 Am^2/kg, a typical value for $CoFe_2O_4$ NPs. [51] Additionally, the *M-H* curve is characterized by a hysteretic behavior (as evidenced in **Figure S1**) with a coercivity of about 22 kA/m and a remanence magnetization of about 8.5 Am^2/kg.

To study the possible use of magnetic hyperthermia to induce radical polymerizations, we chose a model formulation composed of an aqueous solution of acrylamide, the N,N'-metilen-bis-acrylamide (called later only bis-acrylamide) as cross-linker, and the ammonium persulfate (APS) as thermal initiator. The composition was selected to be stable at room temperature for several hours (without observing spontaneous polymerization). The material was chosen for its widespread application, from biological studies (e.g. as support for electrophoresis or cell scaffold) [52,53] to water remediation. [54] The versatility of this formulation allows to achieve different mechanical properties (by modulating the monomer concentration) and to use different polymerization conditions (changing APS concentration or adding some co-initiators). [53]

The solution was subjected to different treatments to achieve the polymerization as shown in Figure 2D. In particular, the formulation was placed within a heating bath (at 60 °C) or exposed to an AC magnetic field with a frequency of 100 kHz. In **Figure S2**, a schematic of the experimental setup for magnetic field application is shown. In each case, if a successful polymerization was obtained, this was qualitatively detected by a simple vial inversion test, since the radical reaction led to a (solid) gel-like material. First, the formulation was exposed to 100 kHz magnetic fields with different peak amplitudes up to the application of a 40 kA/m field for 30 min. No polymerization was observed since the solution remained liquid in all the tests. As expected, we demonstrated that the use of AC magnetic fields without appropriate susceptors is not a useful way to control radical polymerization, due to the negligible eddy current effects. On the other hand, using a standard heating bath, a gel material was obtained. The concentration of APS was

modulated to obtain a complete polymerization in 10 min of reaction at 60 °C, and all the hydrogels, indicated later as prepared by bulk heating, were obtained with this protocol.

The same experiment was repeated by adding the MNPs to the formulation. In this case, magnetic hyperthermia was successful in preparing a hydrogel. In this example, 14 mg/mL of MNPs were added to achieve a complete polymerization in 7 min of application of a 40 kA/m field, as demonstrated by the vial inversion test (Figure 2E). The temperature profile was monitored during the polymerization and an exemplificative trace is reported in Figure 2F. After switching on the field, the temperature increased almost linearly until 60 °C (reached in about 5.8 min), then around 6.8 min a sharper increase was detected, likely due to the heat released by the polymerization exothermic process [55], reaching a maximum of 75 °C. The field was switched off after 7.2 min, when the solid hydrogel was already formed.

Beside the vial inversion test, a successful polymerization was also demonstrated by the Attenuated Total Reflectance (ATR) FTIR spectroscopy (examples are reported in **Figure S3**). In this analysis, the disappearance of the typical band of the acrylamide group, such as the C=C bending at 816 cm^{-1}, was considered as a proof for complete polymerization.

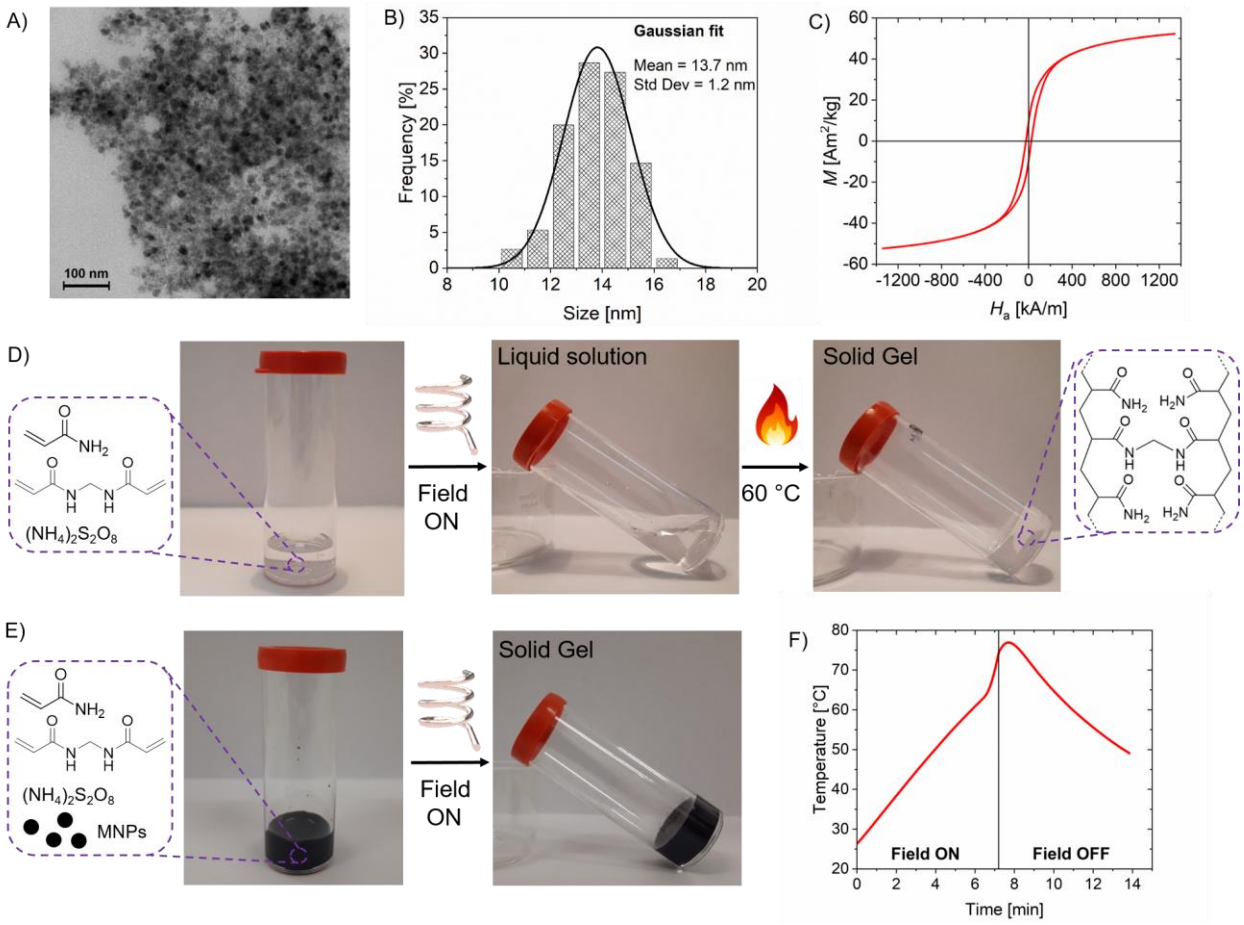

Figure 2. Proof-of-concept for the use of magnetic hyperthermia to trigger radical polymerization. A) A representative TEM image of the MNPs used; B) MNP size distribution histogram derived from statistical analysis of TEM image; C) Static hysteresis loop at room temperature of MNPs; the magnetization value is normalized to the mass of the magnetic material; D) Pictures of the initial hydrogel formulation (left), and the same after AC magnetic field application (center) or immersion in a heating bath at 60 °C (right). The picture in the center shows a liquid material during the vial inversion, revealing no polymerization. The picture on the right demonstrates the formation of a solid hydrogel after standard heating; E) Pictures of the initial hydrogel formulation doped with MNPs (left) and the same after AC magnetic field application (right). In this case, the pictures demonstrate the formation of a solid material during the vial inversion; F) Time evolution of the temperature in a formulation containing the MNPs, during the AC magnetic field exposure and after its switching off.

3.2. Modeling of thermal process and comparison of heating performance of different magnetic nanoparticles

To provide an interpretation of the experimental results, the heating-cooling transient during the magnetic hyperthermia induced polymerization was numerically simulated with the heat transfer model described in the Experimental Part. We used as inputs the SLP of the $CoFe_2O_4$ NPs, derived from thermometric measurements, and the enthalpy change associated with the polymerization reaction obtained with Differential Scanning Calorimetry. [56,57] The heating efficiency of the $CoFe_2O_4$ NPs was estimated by fitting the initial slope of the heating curve (Figure 2F), to calculate the SLP, which is approximately 60 W/g.

Figure 3A shows the time evolution of the temperature, calculated at different points within the magnetic gel (see Figure 3B for their positions). The modeling results are in very good agreement with the experimental ones, with an accurate reproduction of the main phenomena occurring in the solution. During the first part of the transient there was a temperature increase governed by the activation of the MNPs, consequent to the application of the AC magnetic field. After 6 min, when the temperature in the solution reached 60 °C, the exothermic reaction started, leading to a further rise in the temperature curve slope, followed by a decrease at about 7.2 min, when the AC magnetic field is switched off and the heat release from MNPs stops. The temperature continues to increase up to 7.7 min, when the peak of the polymerization enthalpy was reached, then the cooling transient started, with a temperature decrease of about 25 °C in 6 min.

Figure 3B illustrates the temperature map calculated within the magnetic gel in correspondence of the temperature peak, when the heat released by the exothermic reaction is maximal. A small

temperature gradient is observed, with a variation in the order of 1.2 °C in a 3.5 mm sized volume, centered with the sample barycenter.

Thanks to the heat transfer model, we can investigate how the polymerization process can be optimized, by varying the type of MNPs, their concentration in the solution and the AC magnetic field parameters (peak amplitude $\hat{H}_a$ and frequency *f*). As a first result, Figure 3C shows the time interval required to reach the temperature of 60 °C as a function of Q_{MNPs}, i.e. the specific heating power released by MNPs under the action of an AC magnetic field. The value marked with the red circle corresponds to the data used to reproduce the experimental results; in particular, in this case around 6 min of magnetic hyperthermia application are sufficient to trigger the polymerization. This time interval can be properly reduced, by increasing the factors that concur to Q_{MNPs}, namely the MNP SLP (depending on the MNP type and/or on the excitation parameters) and their concentration. As an example, Figures 3D-G compare, in terms of time interval required to reach 60 °C in the same setup previously considered, two types of commercial iron oxide NPs. These are core-shell NPs with citrate shell from NanoMaterials Technology Pte Ltd (known as JHU NPs), and matrix-based NPs constituted by superparamagnetic iron oxide NPs dispersed in a dextran matrix, from micromod Partikeltechnologie GmbH (known as nanomag®-D-spio). [58] Their heating properties, also tested through *in silico* simulations of magnetic hyperthermia applied to murine models, [59] are available from the literature in terms of SLP versus $\hat{H}_a$ and *f*. [35] In particular, for JHU NPs, when *f* = 150 kHz, the SLP varies between 150 and 480 W/g in the range of $\hat{H}_a$ 10−40 kA/m, while, when *f* = 300 kHz, the SLP varies between 50 W/g and 780 W/g in the range of $\hat{H}_a$ 5−20 kA/m. For nanomag®−D−spio NPs, when *f* = 150 kHz, the SLP varies between 15 W/g and 45 W/g in the range of $\hat{H}_a$ 10−40 kA/m, while, when *f* = 300 kHz, the SLP varies between 15 and 70 W/g in the range of $\hat{H}_a$ 5−20 kA/m. As a result

of the different heating properties, MNP concentrations in the order of 5 mg/mL are potentially sufficient for reaching 60 °C and activating the polymerization in 2 min when using JHU NPs and AC magnetic fields with f = 150 kHz and $\widehat{H}_a$ = 40 kA/m (Figure 3D). Even lower concentrations (around 3 mg/mL) and magnetic field peak amplitudes (20 kA/m) are enough when f = 300 kHz (Figure 3E). On the contrary, when using nanomag®-D-spio NPs larger concentrations are needed. In this case, to trigger the polymerization at 60 °C in 2 min, when f = 150 kHz and $\widehat{H}_a$ = 40 kA/m, values around 40 mg/mL have to be considered (Figure 3F), while when f = 300 kHz and $\widehat{H}_a$ = 20 kA/m, the concentration should be at least 30 mg/mL.

To summarize, this model furnishes a roadmap to optimize the polymerization process, providing indication on how to reduce the polymerization time (thanks to a faster heating) by properly selecting the MNP type and their concentration, and the AC magnetic field parameters for the MNP activation.

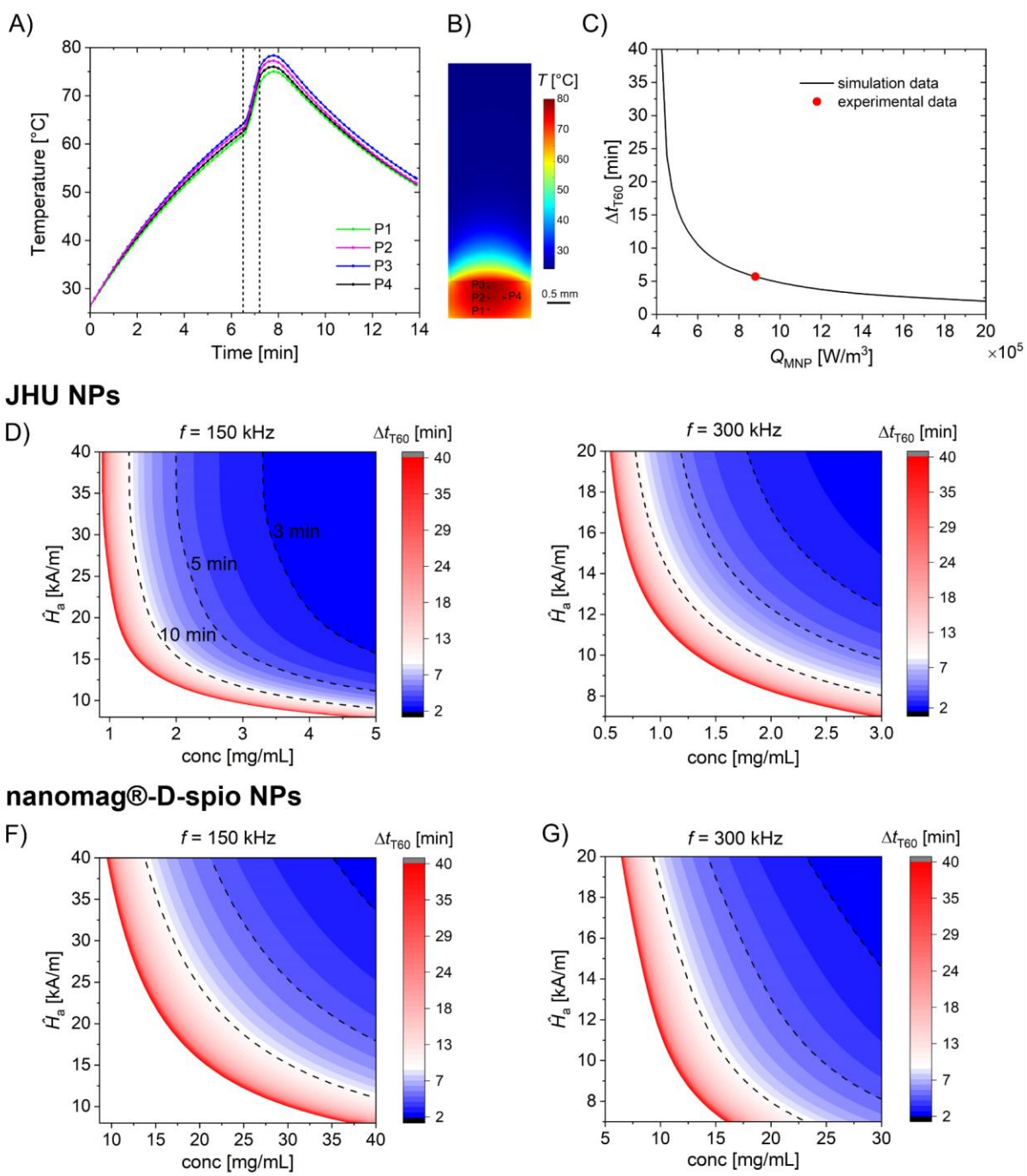

Figure 3. Magnetic nanoparticles used to induce the radical polymerization. A) Simulated heating-cooling transients at different points within the sample, whose positions are marked in the map of Figure B. The time instants corresponding to the polymerization reaction start and the AC magnetic field switching off are indicated with dashed lines. B) Spatial distribution of the temperature calculated on the longitudinal section of the vial at the temperature peak, associated with the maximal enthalpy change during the

polymerization reaction. C) Time interval required to reach 60 °C, as a function of the specific heating power released by MNPs (the experimental data is indicated with a red circle as a reference). Diagrams of the time interval required to reach 60 °C, as a function of MNP concentration and magnetic field peak amplitude, when using commercial MNPs, namely JHU NPs (panel D for f = 150 kHz and panel E for f = 300 kHz) and nanomag®-D-spio NPs (panel F for f = 150 kHz and panel G for f = 300 kHz).

3.3. Hydrogel characterization and possible application of the magnetic hyperthermia induced polymerization

To assess how the presence of the MNPs or the polymerization conditions influence the final hydrogel properties, a characterization was performed by gravimetric methods and rheological tests on 3 hydrogels: two materials containing the $CoFe_2O_4$ NPs and prepared respectively by magnetic hyperthermia or standard bulk heating, and the hydrogel without MNPs (prepared by bulk heating). The magnetic properties of the two magnetic hydrogels were also characterized by means of vibrating sample magnetometry (VSM).

Starting from the gravimetric analysis, the value of gel fraction and swelling degree are summarized in Table 2. The first parameter represents the percentage of the monomer mixture that has successfully undergone polymerization, while the second estimates the maximum amount of water that can be contained in the final materials. In all cases, a gel fraction above 96% was measured, thus demonstrating an almost quantitative polymerization and no inhibition of the radical process by the presence of the MNPs. Considering the hydrogels prepared by bulk heating, we can observe how the introduction of the MNPs led to a slight decrease in the gel fraction (from 98 to 96%) which also corresponds to a small increase in the swelling degree. On the other hand,

comparing the magnetic hydrogels, even if the gel fraction was the same, the swelling degree was reduced by about 5% in the sample prepared by magnetic hyperthermia. This data suggested that a different hydrogel structure was formed during the different polymerization processes leading also to different mechanical properties, as reported in **Figure 4A**-**B**. With respect to similar hydrogel previously investigated by some of us, [53] we observed that a higher amount of APS leads to an increase in gel fraction and a consequent reduction of the swelling capabilities.

Table 2. Parameters obtained by gravimetric characterization of the hydrogels.

Hydrogel	**MNPs**	**Type of polymerization**	**Gel fraction (%)**	**Swelling degree (%)**
1	Yes	Magnetic hyperthermia	96.1	84.4
2	Yes	Bulk heating	96.3	89.6
3	No	Bulk heating	98	86.3

Oscillatory shear measurements also provided evidence of robust gel formation (Figure 4A). Irrespective of the polymerization conditions, indeed, all the samples exhibited a typical gel-like behavior, which is characterized by almost frequency-independent viscoelastic shear moduli, with the elastic modulus, G', being much higher than the viscous one, G''. More information on the effect of the different polymerization conditions can be sought by focusing on the elastic modulus, as it is related to the chemical nature of the polymeric network and to the crosslinking density. [60]

On the one hand, no significant differences can be appreciated for the samples obtained by bulk heating, even in the presence of MNPs, suggesting that the latter did not play any significant role in the thermal-triggered polymerization process. On the other hand, an increase in the elastic contribution can be appreciated in the case of magnetic hyperthermia polymerization. Since the gel fraction is the same as for the sample obtained by bulk heating (see Table 2), the effect of a higher crosslinking density can be ruled out. Hence, the higher G' can be likely ascribed to the formation of a more homogenous crosslinked mesh (no effect of temperature gradients as for bulk heating), in which the MNPs are better integrated in the polymeric matrix. This is in line with the lower swelling degree of the gel obtained by magnetic hyperthermia polymerization, which also suggests the formation of a stiffer network.

Unconfined compression tests further support this picture. Figure 4B shows that magnetic hyperthermia induced polymerization leads to the most mechanically robust gel, which is characterized by a higher elastic modulus, E_c, and higher strength at larger deformation. Interestingly, with respect to the neat gel, both the gels with MNPs possess a higher E_c in spite of a lower gel fraction (see inset), suggesting that the presence of the MNPs plays a role in improving the mechanical resistance under compression. Overall, the measured mechanical properties of the gels are summarized in Table 3.

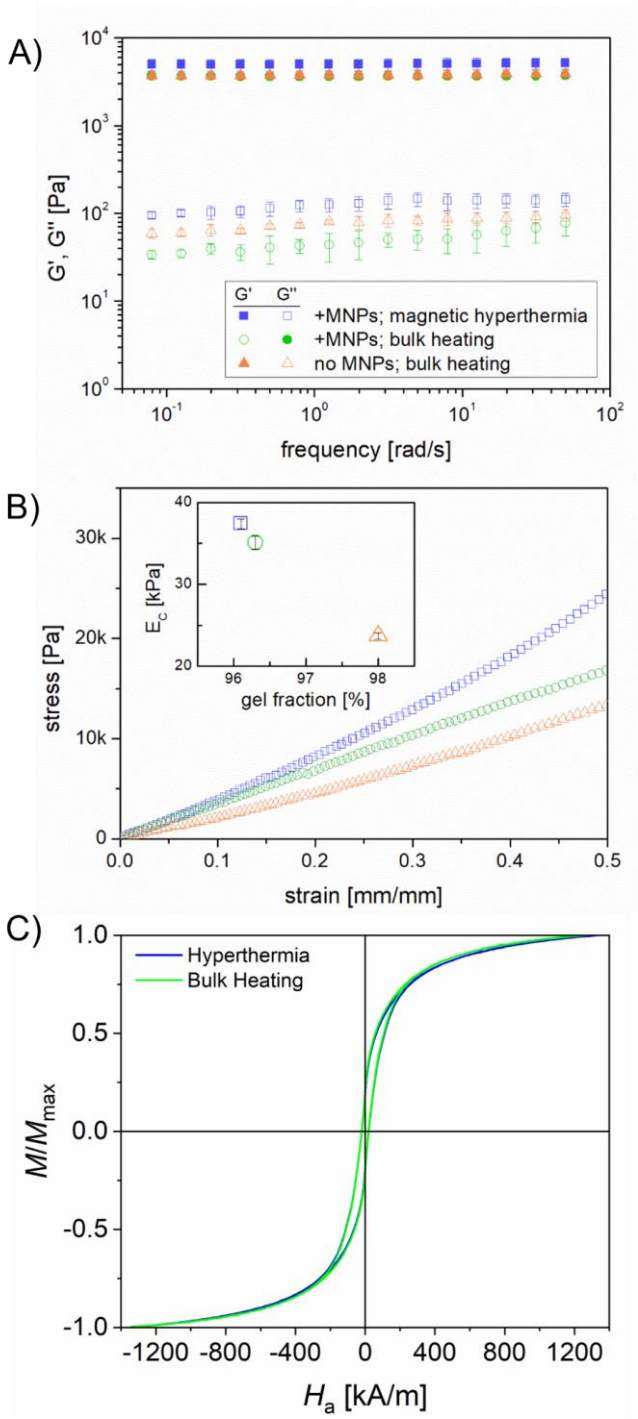

Figure 4. Hydrogel characterization. Rheological and mechanical tests on hydrogels with or withoutMNPs inside: A) frequency dependence of the viscoelastic shear moduli; B) stress-strain curves for unconfined compression. C) Static hysteresis loops at room temperature of magnetic hydrogels prepared by magnetic hyperthermia induced heating or standard bulk heating.

Table 3. Summary of the mechanical properties of the hydrogels

Hydrogel	MNPs	Type of polymerization	G' @ 1 rad/s [kPa]	E_c [kPa]
1	Yes	Magnetic hyperthermia	4.95±0.75	37.4 ± 0.6
2	Yes	Bulk heating	3.71 ± 0.38	35.1 ± 0.8
3	No	Bulk heating	3.64 ± 0.31	23.7 ± 0.4

Comparing the magnetic properties of the hydrogels containing the MNPs, they appeared to be almost identical despite the different initiation of polymerization. This featurewas confirmed by Figure 4C, where the *M-H* curves obtained with VSM at room temperature perfectly overlap.

The overall picture of the characterizations demonstrated that the polymerization induced by magnetic hyperthermia has an impact on the material properties, but its effect is greatly lower than those possibly obtained by modulating the formulation (e.g. concentration of monomers or initiator). [61] Indeed, we have to consider that the application of magnetic hyperthermia resulted in a more complex/more specialized protocol for hydrogel preparation. However, taking advantage of the peculiar characteristic of MNPs, the use of AC magnetic fields to control polymerization reactions could open the way to different opportunities than classical polymerization strategies. Some examples are reported in **Figure 5** and **Figure 6**.

In the first case, the possibility of confining heating preferentially in a selected volume (where a certain amount of MNPs was localized) was exploited to obtain the polymerization in environments that, for example, cannot be heated above a certain temperature (i.e., standard thermal heating is forbidden) or in opaque media (i.e., photopolymerization is not possible). A practical example should be the injection of a polymerizable mixture inside a biological organism and the following *in situ* reaction [11b] induced with a contactless magnetic field application.

In this proof-of-concept, we employed an ultra-low gelling point agarose hydrogel as a thermo-sensitive environment. This material is a physical hydrogel where a 1% w/w solution of agarose was homogenized by heating and became gel at room temperature. The selected agarose allowed for the hydrogel melting around 50 °C, thus employing this material in combination with the bulk thermal heating polymerization previously shown is not possible.

Pictures of the different steps to achieve selective volume polymerization by magnetic hyperthermia are shown in Figure 5. First, a vial was filled with the hot agarose solution and then gelled at room temperature around a (conical) mold. Once removed, we obtained an agarose hydrogel shell (Figure 5A) and the empty (conical) space was filled with the magnetic acrylamide formulation (Figure 5B). Then, different heating treatments were applied. Using a thermal bath at 60 °C, the agarose shell was melted causing the mixing of both the hydrogel formulations before the acrylamide polymerization. Once the system was cooled at room temperature, we observed only the formation of a homogeneous hydrogel with MNPs on the vial bottom or dispersed randomly in the hydrogel (Figure 5C). This experiment confirmed how classical heating cannot be used to achieve a spatial selectivity for the polymerization.

On the other hand, different magnetic hyperthermia treatments were tested until reaching only the polymerization of the acrylamide mixture. In Figure 5D, different examples of successful polymerization of the magnetic formulation without melting the agarose are shown. In this way, the hydrogel maintained the shape adopted by the monomer mixture before the AC magnetic field application and the two materials were not mixed at the end.

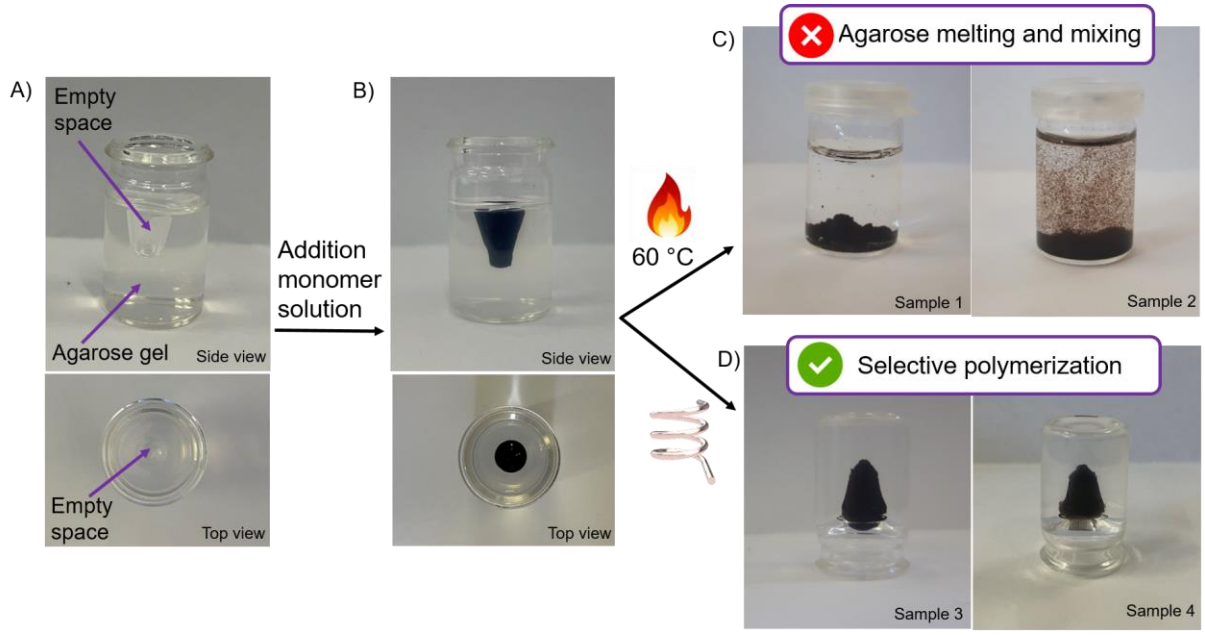

Figure 5. Possible application to induce polymerization in thermo-sensitive environments. An ultra-low gelling temperature agarose hydrogel shell (A) was filled with the acrylamide formulation (B). The samples were subjected to: C) heating in a thermal bath (obtaining agarose melting and mixing of the materials); D) magnetic hyperthermia (to achieve selective acrylamide polymerization). The vial inversion showed the formation of a solid hydrogel.

It is interesting to note that the agarose environment strongly modified the heat dissipation of the systems with respect to the hydrogels presented in Figure 2 and, to achieve the polymerization, a

stronger magnetic field application was necessary (56 kA/m for 20 min). An example of the temperature profile measured in the center of the acrylamide solution during the field application is reported in **Figure S4**. The result demonstrated the influence of the environment on the MNP heating performance, since a maximum temperature of 65 °C was obtained only after 20 min of field application.

As can be observed, all the examples reported up to now where magnetic hyperthermia is exploited lead always to magnetic hydrogels. Indeed, this class of materials can be used for several applications, from biological (e.g. drug delivery, hyperthermia agents in biological systems) [62,63] to environmental one (e.g. oil-water separation, adsorption of water pollutants). [64,65]

If the presence of magnetic nanoparticles in the final material is not desired, they can be removed by selective dissolution, for example by using strong acids (a representative proof-of-concept is given in Figure S5). However, other smarter strategies can be pursued to further enlarge the applicability of magnetic hyperthermia, also for the preparation of materials that do not incorporate MNPs. The concept followed is depicted in Figure 6A: the heating locally released by MNPs that are concentrated in a small volume of the monomeric formulation is exploited to polymerize the whole volume. This case can be seen as a complementary condition to the ones reported in Figure 5, in which by playing on MNP concentration and field application we demonstrated spatially selective heating.

In this example (Figure 6B), the monomer formulation was first doped with a small amount of MNPs (1.4 mg). The new mixture was not able to polymerize during field application under the conditions previously cited (as an effect of the low MNP concentration). Then, the MNPs were collected (with the use of a permanent magnet) only on one side of the formulation and the AC

magnetic field was then applied. After the application for 20 min of a 56 kA/m field, the complete polymerization of the liquid volume was observed. Very interestingly, the heat produced only on one side of the vial can be enough (using appropriate exposure time) to polymerize different material volumes. In our examples, 1.4 mg of MNPs were able to polymerize from 2 to 6 mL of acrylamide solution in 20 min. Indeed, even if the use of a larger amount of well dispersed MNPs (e.g. as in Figure 2) allowed to decrease the necessary field amplitude and the reaction time, the last experiments demonstrated the possibility of obtaining non-magnetic materials by indirect heating, produced by MNPs concentrated in a restricted space.

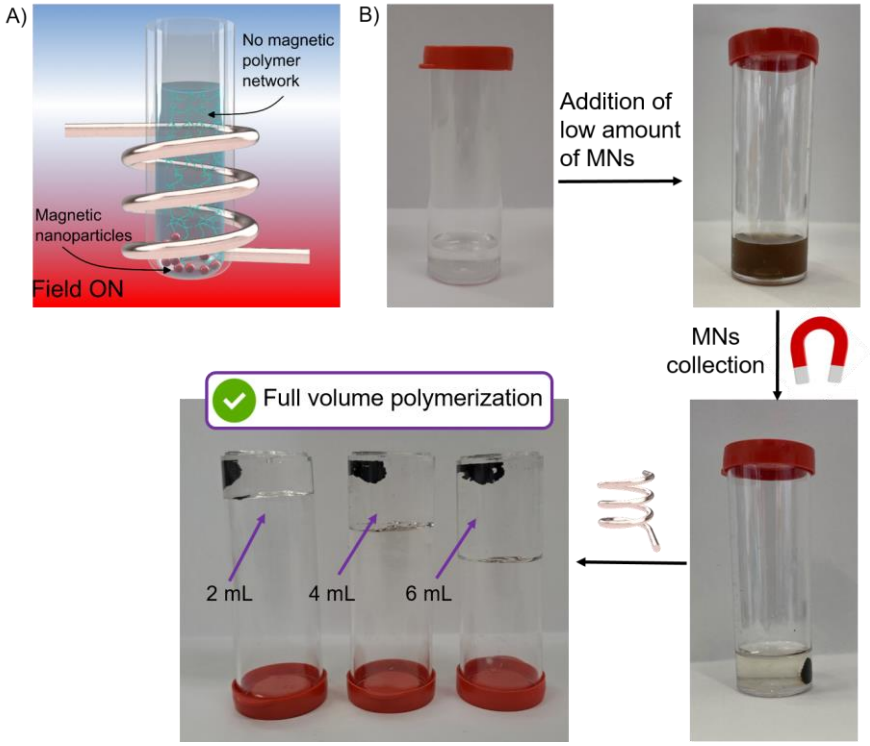

Figure 6. Possible application to prepare non-magnetic hydrogels. A) Scheme of polymerization due to magnetic hyperthermia obtained with MNPs concentrated on the bottom of the vial. B) Sequence of pictures showing the protocol followed to obtain non-magnetic hydrogels polymerized by the action of the MNPs concentrated on one side of the sample.

To investigate the effect of this process on the features of the obtained hydrogel, the 6 mL sample of Figure 6 (i.e., the one having the larger volume) was selected for further analyses. Specifically, after removing the bottom part in which the MNPs wereconfined, the remaining hydrogel was sliced into two equally sized disk-shaped samples that were subsequently characterized by rheological tests. The results are shown in Figure 7, in which the measured properties of the hydrogel obtained by simple bulk heating are also reported for the sake of comparison. It can be noticed from rheological and mechanical tests that the properties of the two hydrogel slices are comparable, suggesting that the polymerization triggered by the confined MNPs proceeds uniformly throughout the sample, at least for the investigated volumes. Moreover, both the elastic shear modulus G' and elastic compression modulus E_c are comparable to those of the hydrogel obtained by simple bulk heating, indicating the reliability and applicability of the proposed approach.

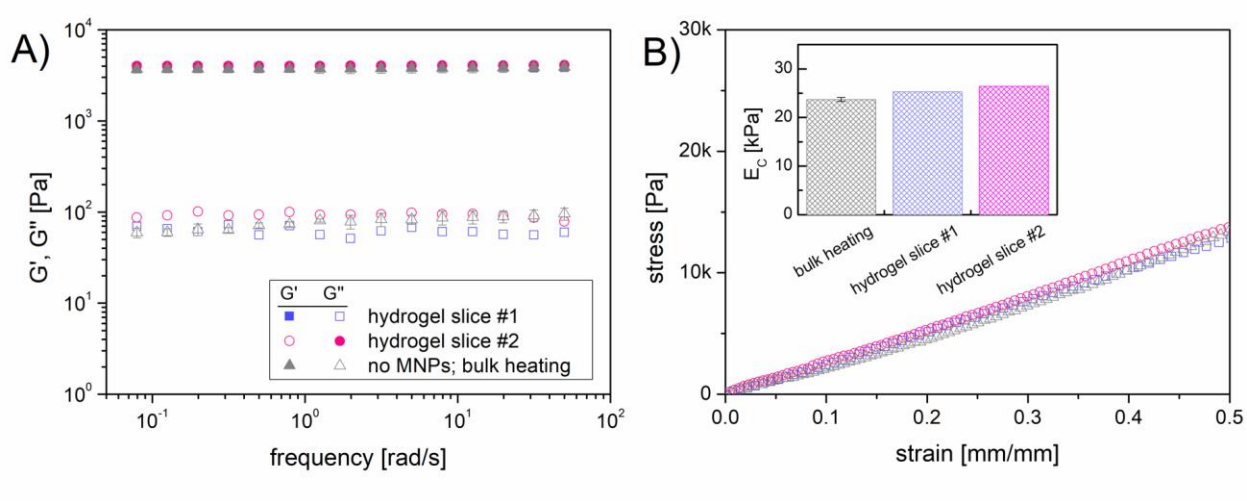

Figure 7. Rheological and mechanical tests on non-magnetic hydrogels obtained by magnetic hyperthermia induced polymerization with confined MNPs. A) Frequency dependence of the

viscoelastic shear moduli; B) stress-strain curves for unconfined compression (the computed elastic modulus is reported in the inset). “Gel slice#1” refers to the top slice, while “Gel slice#2” refers to the slice more in proximity to the MNPs. Data for the reference hydrogel obtained by simple bulk heating are the same as in Figure 4.

Further mechanistic insights were studied and reported in **Figure S6**. First of all, we demonstrated that in all our experimental procedures, MNPs are essential to obtain the acrylamide reaction. Figure S4A showed two vials containing 2 mL of monomer mixture after the same field application (56 kA/m for 20 min). Only if MNPs were present in the formulation, the polymerization occurred and a solid material was formed. If MNPs were not present, the formulation was still liquid as detected by vial inversion. Second, if the heat was mainly generated around the MNPs, a selected polymerized volume around them should be observed for short field application. Indeed, in Figure S5B we demonstrated how playing on the field application time, only a partial polymerization around the MNP aggregates was obtained with the formation of a solid hydrogel. To be noted that at this stage a more precise control on the volume partially polymerized and its shape was not possible, but this observation support show the polymerization started around the MNPs.

4. Conclusion

The addition of MNPs in an acrylamide formulation was demonstrated to start the radical polymerization reaction by magnetic hyperthermia under an AC magnetic field. This preparation method led to a small variation of the hydrogel properties with respect to those of the hydrogel produced by standard bulk thermal polymerization, while other parameters are best to be

considered to modulate the material characteristics (e.g. using different cross-linker amounts). Indeed, we demonstrated a good versatility of the polymerization that can be applied, for example, also in thermo-sensitive environments. The test was performed in a simple agarose hydrogel that cannot be heated more than 50 °C but it paves the way for application in more complex environments like the biological one. Towards this objective, a careful investigation should be performed to reduce the amplitude of the applied fields or the MNP content inside the final materials. Very interestingly, the heat released by the MNPs can be exploited also to polymerize non-magnetic hydrogels, if a low amount of MNPs is concentrated in a small volume and exposed to a prolonged field exposure. The heat generated locally is dissipated inside the whole formulation leading to the radical reaction. Also in this case, improvement of the SLP of the MNPs and modulation of the monomer concentration (to obtain higher heat released during the polymerization) should be exploited to achieve a frontal polymerization initiated by an AC magnetic field.

The protocol described here for a specific mixture should be easily applied to any other water based solutions thanks to the possible (good) dispersion of the MNPs in this solvent. In addition, future studies should be conducted to understand how the use of magnetic hyperthermia could be exploited for the preparation of linear polymers. Also organic monomers and solvents should be employed once the MNPs are functionalized (e.g. by oleic acid) to guarantee good dispersion in non-aqueous matrices. At the end, another fundamental aspect might be the substitution of the $CoFe_2O_3$ NPs with other more biocompatible MNPs, towards application in biological systems or environmental remediation.

ASSOCIATED CONTENT

Supporting Information. The Supporting Information is available free of charge and includes: Additional experimental details, materials, and methods, including photographs of experimental setup, ATR spectra of the materials, other pictures demonstrating different examples of polymerization by magnetic hyperthermia.

AUTHOR INFORMATION

Corresponding Author

* Daniele Martella; e-mail: daniele.martella@unifi.it; martella@lens.unifi.it

Author Contributions

M.V. and D.M. performed the experiments, D.M. designed the experiments, M.S. performed the mechanical characterizations, M.V. and A.M. performed the simulations, G.B. and P.T. supported the magnetic characterization, all the authors wrote the manuscript.

Funding Sources

D.M. and M.S. acknowledge MUR for financial support (project PRIN 2022 WATERONIC, number 20227WZXJ3).

ACKNOWLEDGMENT

The authors acknowledge Dr. Rachele Castaldo for TEM images and Dr. Giuseppe Lio for help in the graphic content.

REFERENCES

[1] Matyjaszewski, K.; T. P. Davis, T. P. Handbook of radical polymerization. *Wiley, Hoboken, NJ, USA* **2002**.

[2] Ballard N.; Asua, J. M. Radical polymerization of acrylic monomers: An overview. *Prog. Polym. Sci*. **2018**, 79, 40-60.

[3] Ganglani, M.; Carr, S. H.; Torkelson, J. M. Thermal, rheological, and mechanical properties of a polymer composite cured at different isothermal cure temperatures. *Polymer* **2002**, 43, 2747–2760.

[4] Ilie, N.; Keßler, A.; Durner, J. Influence of various irradiation processes on the mechanical properties and polymerisation kinetics of bulk-fill resin based composites. *J. Dent.* **2013**, 41, 695–702.

[5] Fang, H.; Guymon, C. A. Recent advances to decrease shrinkage stress and enhance mechanical properties in free radical polymerization: a review. *Polym. Int.* **2022**, 71, 596–607.

[6] Chen, M.; Zhong, M.; Johnson, J. A. Light-Controlled Radical Polymerization: Mechanisms, Methods, and Applications. *Chem. Rev.* **2016**, 116, 10167-10211.

[7] Chmielarz, P.; Fantin, M.; Park, S.; Isse, A. A.; Gennaro, A.; Magenau, A. J. D.; Sobkowiak, A.; Matyjaszewski, K. Electrochemically mediated atom transfer radical polymerization (eATRP). *Prog. Polym. Sci.* **2017**, 69, 47–78.

[8] Wiesbrock, F.; Hoogenboom, R.; Schubert, U. S. Microwave-Assisted Polymer Synthesis: State-of-the-Art and Future Perspectives. *Macromol. Rapid Commun.* **2004**, 25, 1739–1764.

[9] Paulusse, J. M. J.; Sijbesma, R. P. Ultrasound in polymer chemistry: Revival of an established technique. *J. Polym. Sci. A Polym. Chem.* **2006**, 44, 5445–5453.

[10] Zhang, J.; Liao, J.; Liu, Z.; Zhang, R.; Sitti, M. Liquid Metal Microdroplet-Initiated Ultra-Fast Polymerization of a Stimuli-Responsive Hydrogel Composite. *Adv. Funct. Mater.* **2023**, 2308238.

[11] a) Price, G. J.; Norris, D. J.; West, P. J. Polymerization of methyl methacrylate initiated by ultrasound. *Macromol.* **1992**, 25, 6447–6454. b) Debbi, L.; Machour, M.; Dahis, D.; Shoyhet, H.; Shuhmaher, M.; Potter, R.; Tabory, Y.; Goldfracht, I.; Dennis, I.; Blechman, T.; Fuchs, T.; Azhari, H.; Levenberg, S. Ultrasound Mediated Polymerization for Cell Delivery, Drug Delivery, and 3D Printing. *Small Methods* **2024**, 2301197.

[12] Fischer, J.; Wegener, M. Three-dimensional optical laser lithography beyond the diffraction limit. *Laser Photonics Rev.* **2013**, 7, 22–44.

[13] Bagheri, A.; Jin, J. Photopolymerization in 3D Printing. *ACS Appl. Polym. Mater.* **2019**, 1, 593–611.

[14] De Bellis, I.; Nocentini, S.; Delli Santi, M. G.; Martella, D.; Parmeggiani, C.; Zanotto, S.; Wiersma, D. S. Two-Photon Laser Writing of Soft Responsive Polymers via Temperature-Controlled Polymerization. *Laser Photonics Rev.* **2021**, 15, 2100090.

[15] Del Barrio, J.; Sánchez-Somolinos, C. Light to Shape the Future: From Photolithography to 4D Printing. *Adv. Opt. Mater.* **2019**, 7, 1900598.

[16] Nocentini, S.; Martella, D.; Parmeggiani, C.; Wiersma, D. S. 3D Printed Photoresponsive Materials for Photonics. *Adv. Opt. Mater.* **2019**, 7, 1900156.

[17] Chartrain, N. A.; Williams, C. B.; Whittington, A. R. A review on fabricating tissue scaffolds using vat photopolymerization. *Acta Biomater.* **2018**, 74, 90–111.

[18] Bynum, S.; Tullier, M.; Morejon-Garcia, C.; Guidry, J.; Runnoe, E.; Pojman, J. A. The effect of acrylate functionality on frontal polymerization velocity and temperature. *J. Polym. Sci. Part A: Polym. Chem.* **2019**, 57, 982–988.

[19] Robertson, I. D.; Yourdkhani, M.; Centellas, P. J.; Aw, J. E.; Ivanoff, D. G.; Goli, E.; Lloyd, E. M.; Dean, L. M.; Sottos, N. R.; Geubelle, P.H.; Moore, J. S.; White, S. R. Rapid energy-efficient manufacturing of polymers and composites via frontal polymerization. *Nature* **2018**, 557, 223–227.

[20] Malik, M. S.; Schlögl, S.; Wolfahrt, M.; Sangermano, M. Review on UV-Induced Cationic Frontal Polymerization of Epoxy Monomers. *Polymers* **2020**, 12, 2146.

[21] Zimmerer, C.; Mejia, C.; Utech, T.; Arnhold, K.; Janke, A.; Wosnitza, J. Inductive Heating Using a High-Magnetic-Field Pulse to Initiate Chemical Reactions to Generate Composite Materials. *Polymers* **2019**, 11, 535.

[22] Ferraro, A.; Lio, G. E.; Hmina, A.; Palermo, G.; Djouda, J. M.; Maurer, T.; Caputo, R.; Tailoring of plasmonic functionalized metastructures to enhance local heating release. *Nanophotonics* **2021**, 10, 3907–3916.

[23] Ye, S.; Cramer, N. B.; Stevens, B. E.; Sani, R. L.; Bowman, C. N. Induction Curing of Thiol–Acrylate and Thiol–Ene Composite Systems. *Macromol.* **2011**, 44, 4988–4996.

[24] Mittal, A.; Roy, I.; Gandhi, S. Magnetic Nanoparticles: An Overview for Biomedical Applications. *Magnetochemistry* **2022**, 8, 107.

[25] Dennis, C. L.; Ivkov, R. Physics of heat generation using magnetic nanoparticles for hyperthermia. *Int. J. Hyperthermia* **2013**, 29, 715–729.

[26] Khizar, S.; Ahmad, N. M.; Zine, N.; Jaffrezic-Renault, N.; Errachid-el-salhi, A.; Elaissari, A. Magnetic Nanoparticles: From Synthesis to Theranostic Applications. *ACS Appl. Nano Mater.* **2021**, 4, 4284–4306.

[27] Abenojar, E. C.; Wickramasinghe, S.; Bas-Concepcion, J.; Samia, A. C. S. Structural effects on the magnetic hyperthermia properties of iron oxide nanoparticles. *Prog. Nat. Sci.: Mater.* **2016**, 26, 440–448.

[28] Vassallo, M.; Martella, D.; Barrera, G.; Celegato, F.; Coïsson, M.; Ferrero, R.; Olivetti, E. S.; Troia, A.; Sözeri, H.; Parmeggiani, C.; Wiersma, D. S.; Tiberto, P.; Manzin, A. Improvement of Hyperthermia Properties of Iron Oxide Nanoparticles by Surface Coating. *ACS Omega* **2023**, 8,2143–2154.

[29] Schmidt, A. M. Electromagnetic Activation of Shape Memory Polymer Networks Containing Magnetic Nanoparticles. *Macromol. Rapid Commun.* **2006**, 27, 1168–1172.

[30] Mohr, R.; Kratz, K.; Weigel, T.; Lucka-Gabor, M.; Moneke, M.; Lendlein, A. Initiation of shape-memory effect by inductive heating of magnetic nanoparticles in thermoplastic polymers. *Proc. Natl. Acad. Sci. U.S.A.* **2006**, 103, 3540–3545.

[31] Yu, C.; Wang, C.; Chen, S. Robust Self-Healing Host–Guest Gels from Magnetocaloric Radical Polymerization. *Adv Funct Materials* **2014**, 24, 1235–1242.

[32] Diodati, L. E.; Liu, S.; Rinaldi-Ramos, C. M.; Sumerlin, B. S. Magnetic Nanoparticles Improve Flow Rate and Enable Self-Healing in Covalent Adaptable Networks. *ACS Appl. Mater. Interfaces* **2023**, 15, 32957–32966.

[33] Liu, C. W.; Qu, C. Y.; Han, L.; Wang, D. Z.; Xiao, W. B.; Hou, X. Preparation of carbon fiber-reinforced polyimide composites via in situ induction heating. *High Perform. Polym.* **2017**, 29, 1027–1036.

[34] Al-Harbi, L.; Darwish, M.; Khowdiary, M.; Stibor, I. Controlled Preparation of Thermally Stable Fe-Poly(dimethylsiloxane) Composite by Magnetic Induction Heating. *Polymers* **2018**, 10, 507.

[35] Urraca, J. L.; Cortés-Llanos, B.; Aroca, C.; Presa, P. D. L.; Pérez, L.; Moreno-Bondi, M. C. Magnetic Field-Induced Polymerization of Molecularly Imprinted Polymers. *J. Phys. Chem. C* **2018**, 122, 10189–10196.

[36] Griffete, N.; Fresnais, J.; Espinosa, A.; Taverna, D.; Wilhelm, C.; Ménager, C. Thermal Polymerization on the Surface of Iron Oxide Nanoparticles Mediated by Magnetic Hyperthermia: Implications for Multishell Grafting and Environmental Applications. *ACS Appl. Nano Mater.* **2018**, 1, 547–555.

[37] Dadashi-Silab, S.; Yar, Y.; Yagci Acar, H.; Yagci, Y. Magnetic iron oxide nanoparticles as long wavelength photoinitiators for free radical polymerization. *Polym. Chem.* **2015**, 6, 1918–1922.

[38] Gao, L.; Zhuang, J.; Nie, L.; Zhang, J.; Zhang, Y.; Gu, N.; Wang, T.; Feng, J.; Yang, D.; Perrett, S.; Yan, X. Intrinsic peroxidase-like activity of ferromagnetic nanoparticles. *Nat. Nanotechnol.* **2007**, 2, 577–583.

[39] Ibeaho, W. F.; Chen, M.; Shi, J.; Chen, C.; Duan, Z.; Wang, C.; Xie, Y.; Chen, Z. Multifunctional Magnetic Hydrogels Fabricated by Iron Oxide Nanoparticles Mediated Radical Polymerization. *ACS Appl. Polym. Mater.* **2022**, 4, 4373–4381.

[40] Kongcharoen, H.; Coester, B.; Yu, F.; Aziz, I.; Poh, W. C.; Tan, M. W. M.; Tonanon, P.; Ciou, J.; Chan, B.; Webster, R. D.; Lew, W. S.; Lee, P. S. Magnetically Directed Co-nanoinitiators for Cross-Linking Adhesives and Enhancing Mechanical Properties. *ACS Appl. Mater. Interfaces* **2021**, 13, 57851–57863.

[41] de Santana, W. M. O. S.; Abramson, S.; Fini, R.; Caetano, B. L.; Ménager, C.; Pulcinelli, S. H.; Santilli, C. V. Ureasil–Polyether–$CoFe_2O_4$ Nanocomposites: Coupling a Drug Delivery System and Magnetic Hyperthermia. *ACS Appl. Polym. Mater.* **2021**, 3, 4837–4848.

[42] Manzin, A.; Ferrero, R.; Vicentini, M. From Micromagnetic to In Silico Modeling of Magnetic Nanodisks for Hyperthermia Applications. *Adv. Theory Simul.* **2021**, 4, 2100013.

[43] Kosky, P.; Balmer, R.; Keat, W.; Wise, G. Exploring Engineering. An introduction to engineering and design. *Academic Press, Oxford, UK* **2020**.

[44] Prokop, A. F.; Vaezy, S.; Noble, M. L.; Kaczkowski, P. J.; Martin, R. W.; Crum, L. A. Polyacrylamide gel as an acoustic coupling medium for focused ultrasound therapy. *Ultrasound Med. Biol.* **2003**, 29, 1351–1358.

[45] Balakrishnan, P. B.; Silvestri, N.; Fernandez-Cabada, T.; Marinaro, F.; Fernandes, S.; Fiorito, S.; Miscuglio, M.; Serantes, D.; Ruta, S.; Livesey, K.; Hovorka, O.; Chantrell, R.; Pellegrino, T. Exploiting Unique Alignment of Cobalt Ferrite Nanoparticles, Mild Hyperthermia, and Controlled Intrinsic Cobalt Toxicity for Cancer Therapy. *Adv. Mater.* **2020**, 32, 2003712.

[46] Ferrero, R.; Manzin, A.; Barrera, G.; Celegato, F.; Coïsson, M.; Tiberto, P. Experimental and Modelling Analysis of the Hyperthermia Properties of Iron Oxide Nanocubes. *Sci. Rep.* **2019**, 9, 6591.

[47] Espinosa, A.; Kolosnjaj-Tabi, J.; Abou-Hassan, A.; Sangnier, A. P.; Curcio, A.; Silva, A. K. A.; Di Corato, R.; Neveu, S.; Pellegrino, T.; Liz-Marzán, L. M.; Wilhelm, C. Magnetic (Hyper)Thermia or Photothermia? Progressive Comparison of Iron Oxide and Gold Nanoparticles Heating in Water, in Cells, and in Vivo. *Adv. Funct. Mater.* **2018**, 28, 1803660.

[48] Albino, M.; Fantechi, E.; Innocenti, C.; López-Ortega, A.; Bonanni, V.; Campo, G.; Pineider, F.; Gurioli, M.; Arosio, P.; Orlando, T.; Bertoni, G.; de Julián Fernández, C.; Lascialfari, A.; Sangregorio, C. Role of Zn^{2+} Substitution on the Magnetic, Hyperthermic, and Relaxometric Properties of Cobalt Ferrite Nanoparticles. *J. Phys. Chem. C* **2019**, 123, 6148–6157.

[49] Roca, A. G.; Gutiérrez, L.; Gavilán, H.; Fortes Brollo, M. E.; Veintemillas-Verdaguer, S.; Morales, M. D. P. Design strategies for shape-controlled magnetic iron oxide nanoparticles. *Adv. Drug Deliv. Rev.* **2019**, 138, 68–104.

[50] Gavilán, H.; Rizzo, G. M. R.; Silvestri, N.; Mai, B. T.; Pellegrino, T. Scale-up approach for the preparation of magnetic ferrite nanocubes and other shapes with benchmark performance for magnetic hyperthermia applications. *Nat. Protoc.* **2023**, 18, 783–809.

[51] Amiri, S.; Shokrollahi, H. The role of cobalt ferrite magnetic nanoparticles in medical science. *Mater. Sci. Eng. C* **2013**, 33, 1–8.

[52] Smithmyer, M. E.; Sawicki, L. A.; Kloxin, A. M. Hydrogel scaffolds as *in vitro* models to study fibroblast activation in wound healing and disease. *Biomater. Sci.* **2014**, 2, 634–650.

[53] Cappitti, A.; Palmieri, F.; Garella, R.; Tani, A.; Chellini, F.; Salzano De Luna, M.; Parmeggiani, C.; Squecco, R.; Martella, D.; Sassoli, C. Development of accessible platforms to promote myofibroblast differentiation by playing on hydrogel scaffold composition. *Biomater. Adv.* 2023, 155, 213674.

[54] Kaşgöz, H.; Özgümüş, S.; Orbay, M. Modified polyacrylamide hydrogels and their application in removal of heavy metal ions. *Polymer* **2003**, 44, 1785–1793.

[55] de Almeida, A. A.; De Biasi, E.; Mansilla, M. V.; Valdés, D. P.; Troiani, H. E.; Urretavizcaya, G.; Torres, T. E.; Rodríguez, L. M.; Fregenal, D. E.; Bernardi, G. C.; Winkler, E. L.; Goya, G. F.; Zysler, R. D.; Lima, E. Magnetic Hyperthermia Experiments with Magnetic Nanoparticles in Clarified Butter Oil and Paraffin: A Thermodynamic Analysis. *J. Phys. Chem. C* **2020**, 124, 27709–27721.

[56] Abu-Thabit, N. Y. Thermochemistry of Acrylamide Polymerization: An Illustration of Auto-acceleration and Gel Effect. *WJCE* **2017**, 5, 94–101.

[57] Kishore, K.; Santhanalakshmi, K. N. Thermal polymerization of acrylamide by differential scanning calorimetry. *J. Polym. Sci., Part A: Polym. Chem.* **1981**, 19, 2367–2375.

[58] Soetaert, F.; Kandala, S. K.; Bakuzis, A.; Ivkov, R. Experimental estimation and analysis of variance of the measured loss power of magnetic nanoparticles. *Sci. Rep.* **2017**, 7, 6661.

[59] Vicentini, M.; Ferrero, R.; Manzin, A. In Silico Experiments to Explore the Heating Efficiency of Magnetic Nanoparticles in Hyperthermia Preclinical Tests. *Adv. Theory Simul.* **2023**, 6, 2300234.

[60] Flory, P. J. Molecular theory of rubber elasticity. *Polymer* **1979**, 20, 1317–1320.

[61] Pelham, R. J.; Wang, Y. Cell locomotion and focal adhesions are regulated by substrate flexibility. *Proc. Natl. Acad. Sci. U.S.A.* **1997**, 94, 13661–13665.

[62] Li, Y.; Huang, G.; Zhang, X.; Li, B.; Chen, Y.; Lu, T., Lu, T. J.; Xu, F. Magnetic hydrogels and their potential biomedical applications. *Adv. Funct. Mater.* **2013**, 23, 660-672.

[63] Meenach, S. A.; Hilt, J. Z.; Anderson, K. W. Poly (ethylene glycol)-based magnetic hydrogel nanocomposites for hyperthermia cancer therapy. *Acta Biomater.* **2010**, 6, 1039-1046.

[63] Singh, R.; Datta, B. Advances in Biomedical and Environmental Applications of Magnetic Hydrogels. *ACS Appl. Polym. Mater.* **2023**, 5, 5474-5494.

[64] Du, R.; Zhao, Q.; Zheng, Z.; Hu, W.; Zhang, J. 3D Self-Supporting Porous Magnetic Assemblies for Water Remediation and Beyond. *Adv. Energy Mater.* **2016**, 6, 1600473.

Table of Contents.